

Supporting Information

Zn–O–C bonds for efficient electron/ion bridging in ZnSe/C composites boosting sodium ion storage

Xu Xie^a, Zhoulan Yin^a, You Li^a, Ruixuan Tu^a, Yang Liu^a, Hui Tong^b, Xingyue Ma^a,
Zhiying Ding^{a*}, and Lijiao Zhou^{c*}

^aSchool of Chemistry and Chemical Engineering, Central South University, Changsha
410083, China, zy.ding@csu.edu.cn

^bSchool of Metallurgy and Environment, Central South University, Changsha, 410083,
China;

^cSchool of Materials Science and Engineering, Northwestern Polytechnical University,
Xi'an 710072, China, zhouljiao@126.com

*Corresponding author

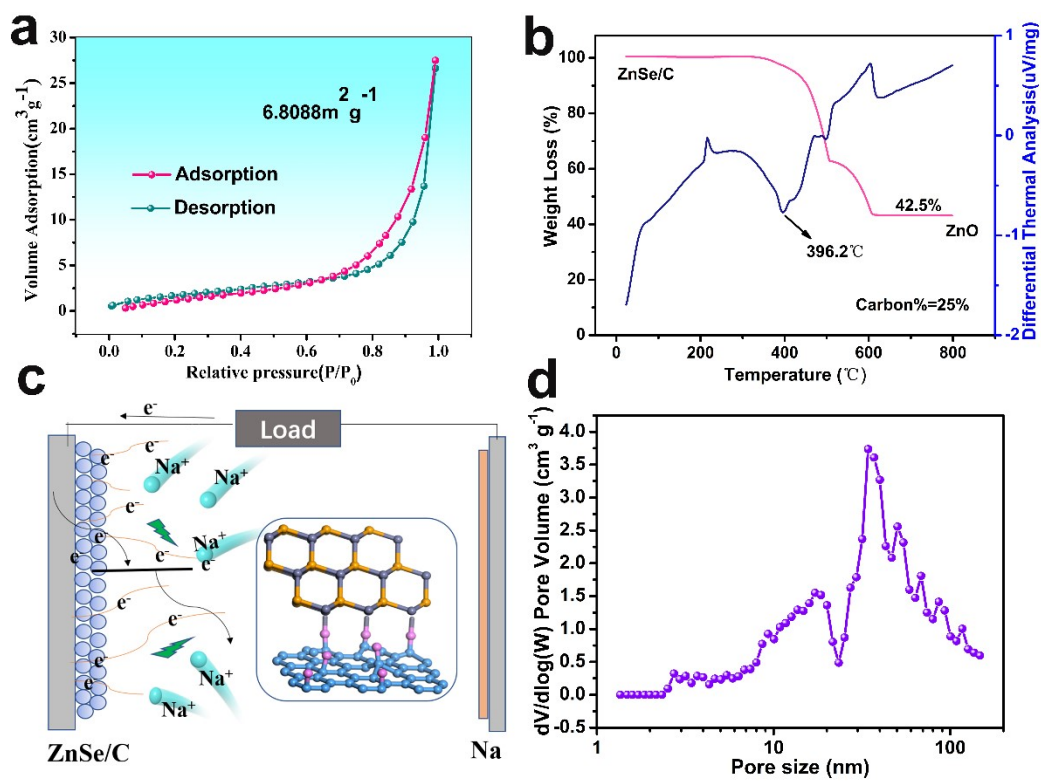


Fig. S1 (a) Nitrogen adsorption/desorption isotherms curve of the ZnSe/C composites, and (b) TG/DTA curves; (c) the mechanism of Zn-O-C bonds accelerate electron transmission. (d) pore size distribution curve of ZnSe/C.

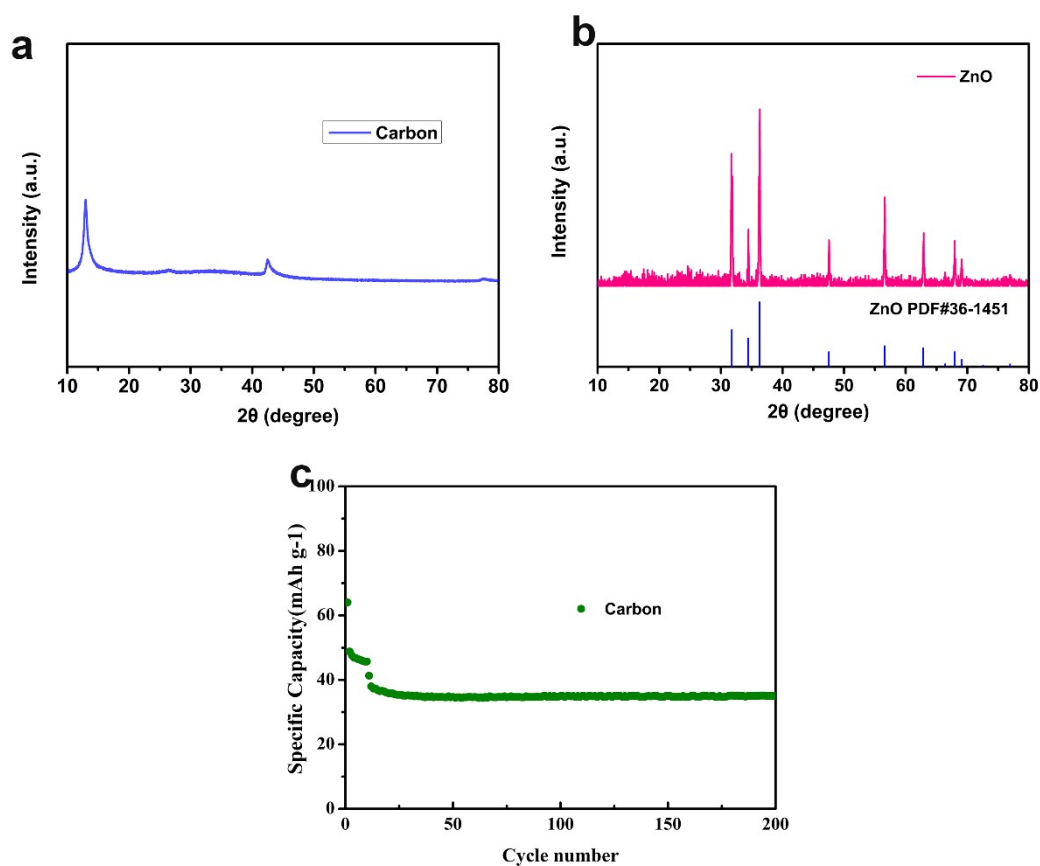


Fig. S2 (a)XRD of Carbon obtained by sintering citric acid. (b)XRD of the products after combustion. (c) Cycling performance of Carbon.

Pure carbon anode material was prepared via one-step sintering. 0.3 g citric acid was fully ground for 1h, then placed in a burning boat and calcined in a tube furnace under mixed hydrogen and argon atmosphere. The calcinations were carried out at a heating rate of 1 °C/min to 300 °C for 3 h. **Fig. S2a** shows the XRD patterns of carbon. The peaks at 12° and 42° were the characteristic peaks of graphene oxide. When it was employed as anode for SIBs, the sodium storage capacity of pure carbon materials prepared by citric acid is only 38 mAh g⁻¹(**Fig. S2c**).

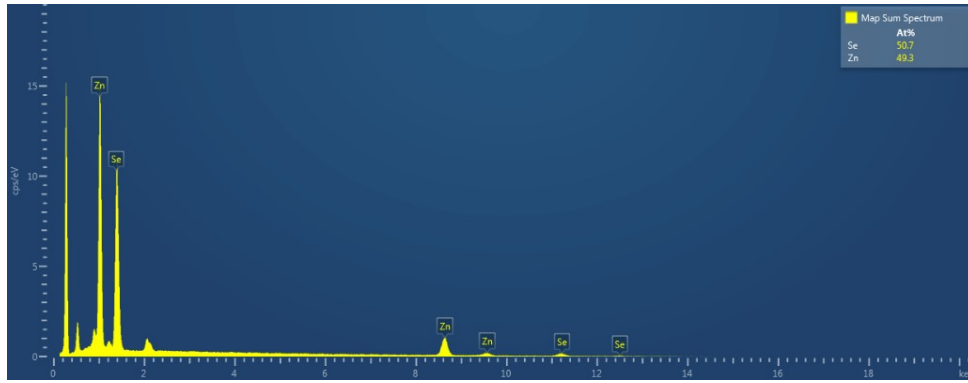


Fig. S3 EDX spectrum of ZnSe/C.

Fig. S3 shows that the ratio of Zn, Se elements in ZnSe@3D is 1 : 1, which further proves that ZnSe was successfully prepared.

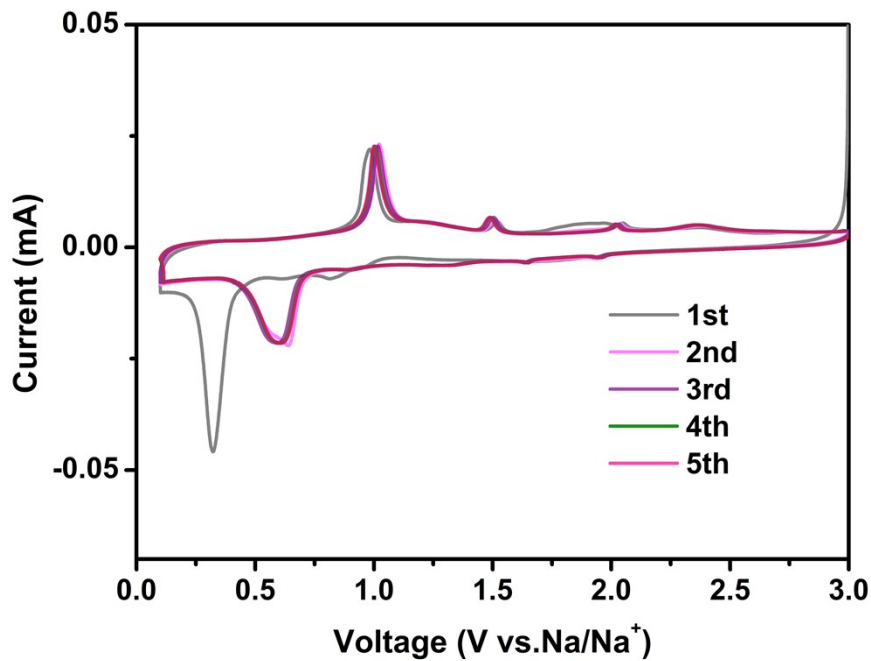


Fig. S4 Initial CV curves of ZnSe/C at a scan rate of 0.1 mV s^{-1}

Fig. S4 shows the initial CV curves of ZnSe/C at a scan rate of 0.1 mV s^{-1} . The first CV curve displays much different shapes from those of the following cycles. Specifically, the cathodic peaks at 1.3 V and 0.6V can be ascribed to the sodium insertion, corresponding to the sequential conversion of ZnSe to metallic Zn and Na_2Se , and then to alloy NaZn_{13} ^{1, 2}. Besides, the appearance of a sharp peak around 0.3 V in the first cycle is indicative of the inevitable formation of a solid electrolyte interface (SEI) film. In the anodic scan, two oxidation peaks at 1.1 and 1.5 V corresponded to the sequential phase transitions of the desodiation process².

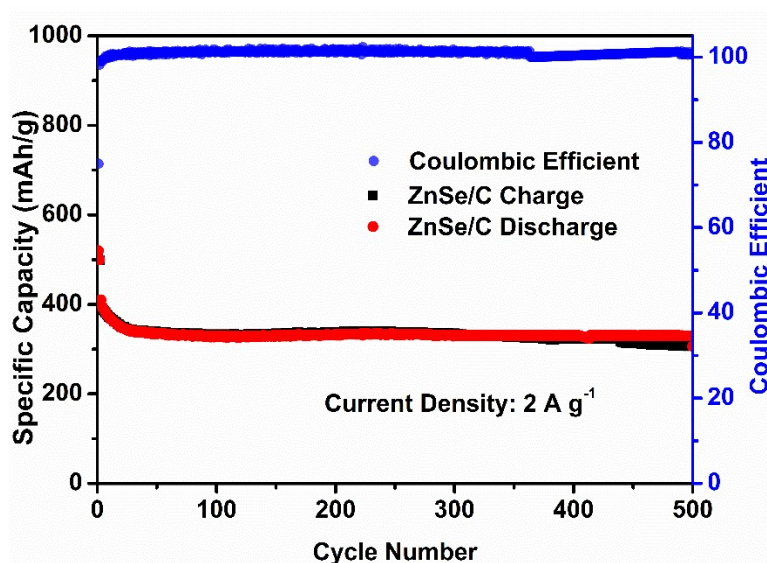


Fig.S5 Cycling performance of ZnSe/C at 2 A g^{-1}

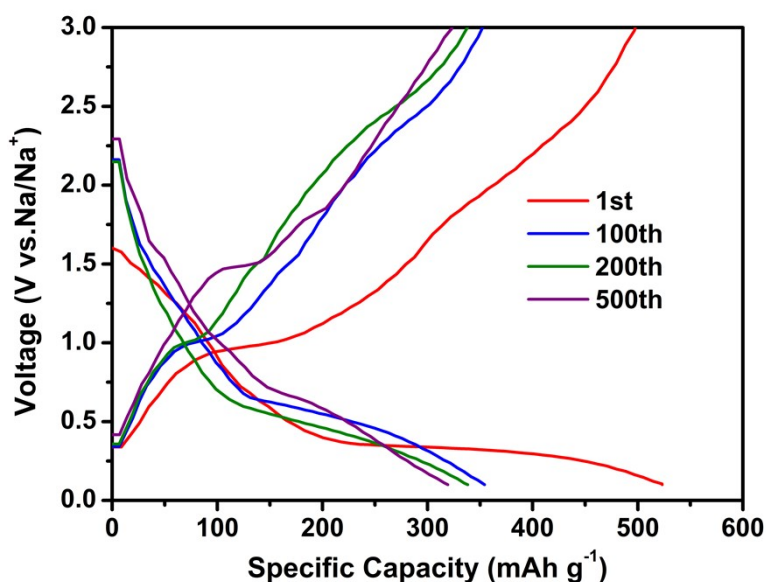


Fig.S6 Galvanostatic discharge/charge profiles of ZnSe/C at 2 A g^{-1} .

Fig. S5 shows the cycling performance of ZnSe/C at a current density of 2 A g^{-1} . ZnSe/C delivers a reversible capacity of 316 mAh g^{-1} after 500 cycles with a coulombic efficiency of almost 100%. For the initial discharge curve, the extended charge plateau at around 0.3 V can be observed, which is due to the formation of the SEI layer(**Fig. S6**). The initial discharge capacity and coulombic efficiency of ZnSe/C are 536 mAh g^{-1} and 73%, respectively. For the next cycles, the charge/discharge profiles show similar shapes, in which the charge/discharge plateau is consistent with the CV curves.

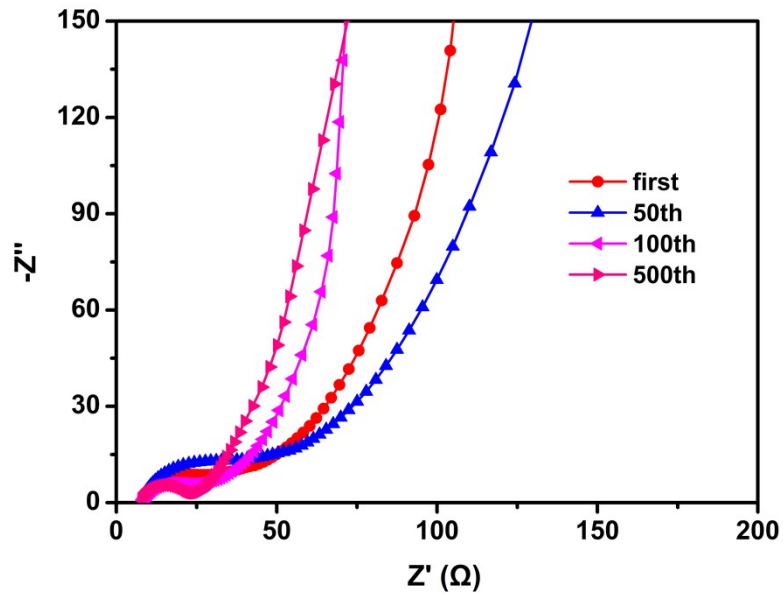


Fig.S7 Nyquist plots at different cycles.

Fig.S7 shows the Nyquist plots at different cycles. The EIS plots are constituted by the internal resistance (R_s), the impedance (R_f) of the electrode/electrolyte interface and the charge-transfer impedance (R_{ct})³. After 50 cycles, the charge transfer impedance reaches the maximum. The increase of charge transfer impedance could be attributed to the formation of thick but unstable SEI film⁴. Then the charge transfer impedance decreases after 100 cycles due to the gradual activation of the active material⁴.

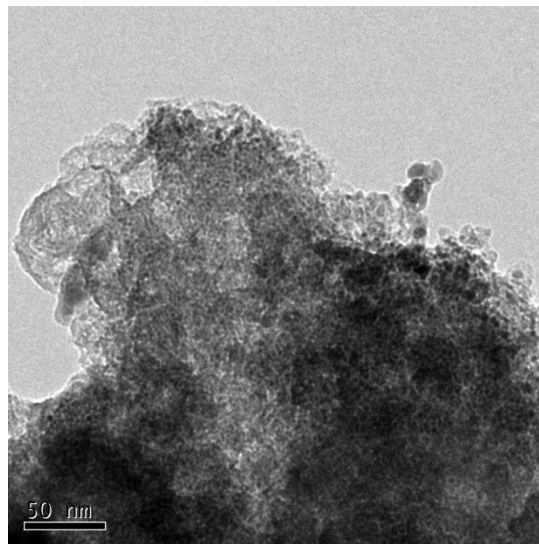


Fig.S8 Ex-situ TEM of ZnSe/C after 500 cycles.

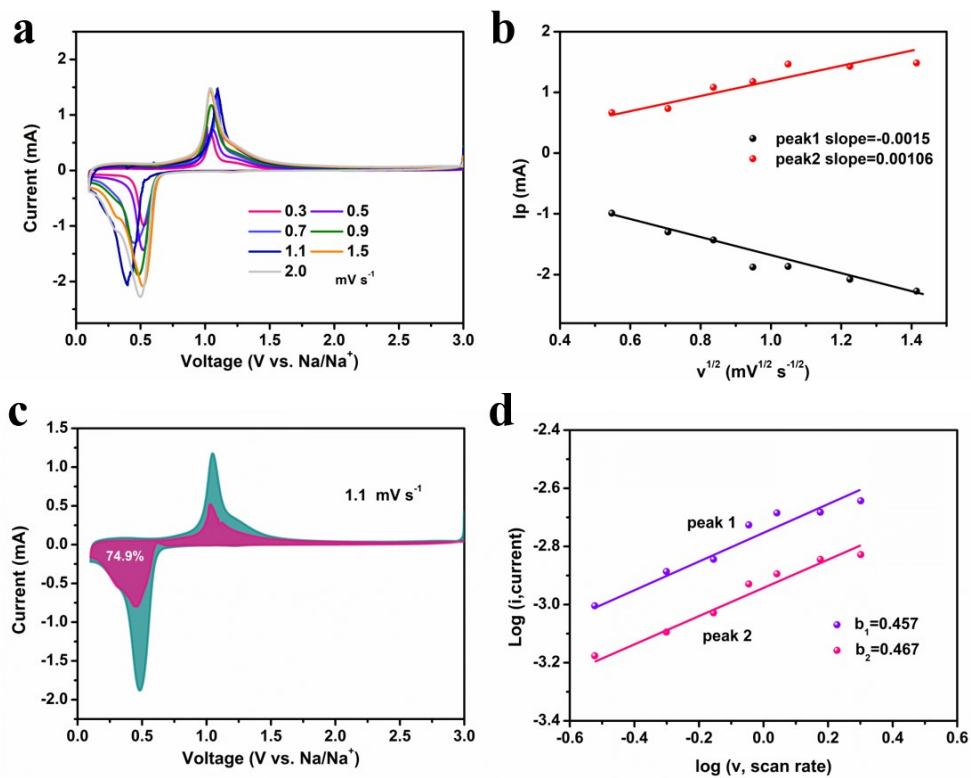


Fig.S9 a) CV curves of bulk ZnSe anode at different sweep rate (0.3–2.0 mV s⁻¹). b) Plots of $v^{1/2}$ vs. I_p . c) CV curve with corresponding capacitive contribution at 1.1 mV s⁻¹. d) the liner of $\log v$ vs. $\log I$ from CV curve.

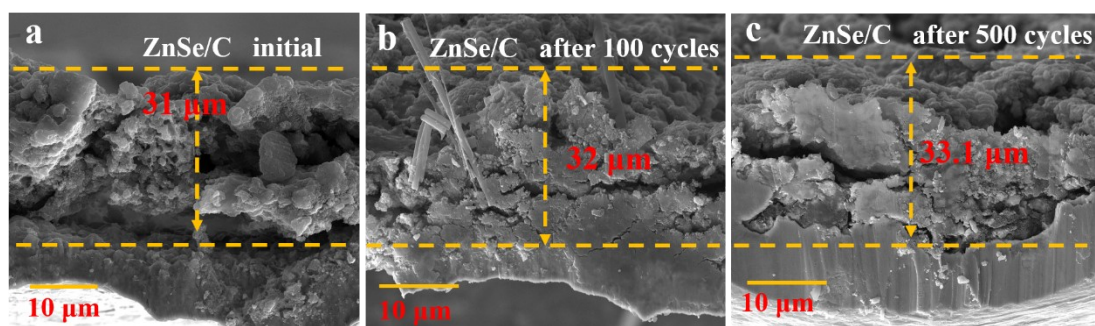


Fig. S10 Thickness change of the ZnSe/C electrodes initial and after 100, 500 cycles.

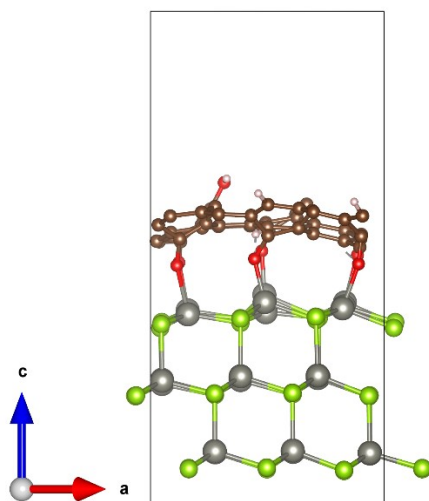


Fig. S11 Structural configurations of ZnSe/C in DFT calculations.

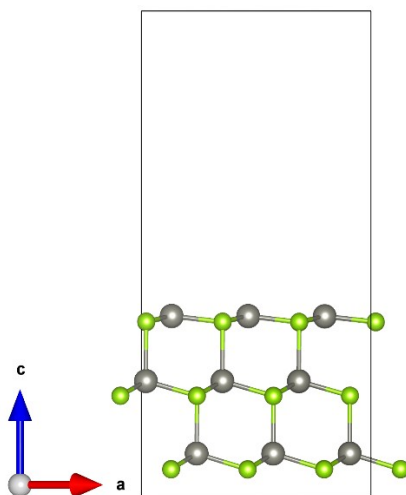


Fig. S12 Structural configurations of ZnSe in DFT calculations.

Table. 1 The comparison of ZnSe and other anodes with remarkable cycling stability employed in SIBs.

Materials	Manner	Electrolyte	Voltage (V)	CE	Current (A g ⁻¹)	Cycle (n)	Capacity mAh g ⁻¹	Ref
ZnSe@NC	solvothormal	CF ₃ NaSO ₃	3.0-0.1	81.95%	0.5	200	311.0	2020 ⁵
ZnSe/ MWCNT	hydrotherma	CF ₃ NaSO ₃	3.0-0.01	88%	0.5	180	382	2018 ⁶
ZnSe@C	Calcining ZIF-8	NaPF ₆	3.0-0.1	81%	0.2	50	389	2019 ⁷
ZnSe-NC@CoSe ₂ -NC	Calcining ZIF-8 · ZIF67	NaClO ₄	3.0-0.005	56.9%	0.1	150	308.5	2019 ⁸
ZnSe@HCNs	hydrotherma	NaPF ₆	3.0-0.1	92.2%	1.0	1000	361.9	2019 ⁹
ZnSe@CoSe/NC	Calcining ZIF-8 · ZIF67	NaClO ₄	2.5-0.1	82%	1.0	1000	273.5	2020 ¹⁰
ZnSe-rGO	hydrotherma	NaClO ₄	3.0-0.1	71%	0.1	50	259.5	2018 ¹¹
ZnSe nanofibers	electrospin	NaCF ₃ SO ₃	3.0-0.01	72%	2.0	200	368.9	2019 ¹²
ZnSe@C@rGO	hydrotherma	NaCF ₃ SO ₃	3.0-0.01	68.1%	0.5	140	243.9	2020 ¹³
ZnSe/MWCNTs	hydrotherma	NaCF ₃ SO ₃	3.0-0.01	59%	4.0	300	281.7	2021 ¹⁴
ZnSe/C	Facile	Facile	3.0-0.1	86.3%	0.5	500	434	This
	Calcining	Calcining			5.0	1000	285	work

Reference

- 1 Y. He, L. Wang, C. Dong, C. Li, X. Ding, Y. Qian and L. Xu, *Energy Storage Mater*, 2019, **23**, 35-45.
- 2 P. Liu, J. Han, K. Zhu, Z. Dong and L. Jiao, *Adv Energy Mater*, 2020, **10**, 2000741.
- 3 S. H. Yang, S.-K. Park and Y. C. Kang, *Chem. Eng. J.*, 2019, **370**, 1008-1018.
- 4 Y. Zhang, P. Chen, Q. Wang, Q. Wang, K. Zhu, K. Ye, G. Wang, D. Cao, J. Yan and Q. Zhang, *Adv Energy Mater*, 2021, **11**, 2101712.
- 5 C. Dong, L. Wu, Y. He, Y. Zhou, X. Sun, W. Du, X. Sun, L. Xu and F. Jiang, *Small*, 2020, **16**, 2004580.
- 6 C. Tang, X. Wei, X. Cai, Q. An, P. Hu, J. Sheng, J. Zhu, S. Chou, L. Wu and L. Mai, *ACS Appl Mater & Interfaces*, 2018, **10**, 19626-19632.
- 7 L. Zeng, Y. Fang, L. Xu, C. Zheng, M. Q. Yang, J. He, H. Xue, Q. Qian, M. Wei and Q. Chen, *Nanoscale*, 2019, **11**, 6766-6775.
- 8 X. Hu, X. Liu, K. Chen, G. Wang and H. Wang, *J Mater Chem A*, 2019, **7**, 11016-11037.
- 9 S. Lu, T. Zhu, H. Wu, Y. Wang, J. Li, A. Abdelkader, K. Xi, W. Wang, Y. Li, S. Ding, G. Gao and R. V. Kumar, *Nano Energy*, 2019, **59**, 762-772.
- 10 Z. Zhang, Y. Huang, X. Liu, X. Wang and P. Liu, *Acs Sustain Chem Eng*, 2020, **8**, 8381-8390.

- 11 X. Cao, A. Li, Y. Yang and J. Chen, *Rsc Adv*, 2018, **8**, 25734-25744.
- 12 P. Zhou, M. Zhang, L. Wang, Q. Huang, Z. Su, L. Li, X. Wang, Y. Li, C. Zeng and Z. Guo, *Front Chem*, 2019, **7**, 569.
- 13 S. Men, H. Zheng, D. Ma, X. Huang and X. Kang, *J. Energy Chem*, 2021, **54**, 124-130.
- 14 Y. Zhou, X. Sun, A. Fan, Y. Shang, K. Xiong, J. Guo, S. Jin, S. Cai and C. Zheng, *Appl. Surf. Sci.*, 2021, **538**, 148194.